Earth Syst. Sci. Data, 13, 923–942, 2021
https://doi.org/10.5194/essd-13-923-2021

Open Access Earth System Science Data

A solar optical hyperspectral library of rare-earth-bearing minerals, rare-earth oxide powders, copper-bearing minerals and Apliki mine surface samples

Friederike Koerting[1], Nicole Koellner[1], Agnieszka Kuras[1], Nina Kristin Boesche[1], Christian Rogass[1], Christian Mielke[1], Kirsten Elger[1], and Uwe Altenberger[2]

[1]GFZ German Research Centre for Geosciences, Potsdam, 14473, Germany
[2]University of Potsdam, Institute of Geosciences, Potsdam, 14476, Germany

Correspondence: Friederike Körting (koerting@gfz-potsdam.de)
and Nicole Koellner (nicolek@gfz-potsdam.de)

Received: 19 November 2019 – Discussion started: 9 December 2019
Revised: 1 February 2021 – Accepted: 2 February 2021 – Published: 9 March 2021

Abstract. Mineral resource exploration and mining is an essential part of today's high-tech industry. Elements such as rare-earth elements (REEs) and copper are, therefore, in high demand. Modern exploration techniques from multiple platforms (e.g., spaceborne and airborne), to detect and map the spectral characteristics of the materials of interest, require spectral libraries as an essential reference. They include field and laboratory spectral information in combination with geochemical analyses for validation. Here, we present a collection of REE- and copper-related hyperspectral spectra with associated geochemical information. The libraries contain reflectance spectra from rare-earth element oxides, REE-bearing minerals, copper-bearing minerals and mine surface samples from the Apliki copper–gold–pyrite mine in the Republic of Cyprus. The samples were measured with the HySpex imaging spectrometers in the visible and near infrared (VNIR) and shortwave infrared (SWIR) range (400–2500 nm). The geochemical validation of each sample is provided with the reflectance spectra. The spectral libraries are openly available to assist future mineral mapping campaigns and laboratory spectroscopic analyses. The spectral libraries and corresponding geochemistry are published via GFZ Data Services with the following DOIs: https://doi.org/10.5880/GFZ.1.4.2019.004 (13 REE-bearing minerals and 16 oxide powders, Koerting et al., 2019a), https://doi.org/10.5880/GFZ.1.4.2019.003 (20 copper-bearing minerals, Koellner et al., 2019), and https://doi.org/10.5880/GFZ.1.4.2019.005 (37 copper-bearing surface material samples from the Apliki copper–gold–pyrite mine in Cyprus, Koerting et al., 2019b). All spectral libraries are united and comparable by the internally consistent method of hyperspectral data acquisition in the laboratory.

1 Introduction

Reflectance spectroscopy is based on measuring the reflected solar radiation from a material of interest. It uses photosensitive detectors to record and analyze light reflected or scattered from the surface. The spectrum of the reflected light is unique for each material and acts like a spectral fingerprint. Spectral libraries are comprehensive collections representing optical properties of materials in a specific wavelength range. In this data collection, hyperspectral spectra were collected under standardized laboratory or field conditions and include geochemical analyses of the sampled minerals and materials. The geochemical analyses can be used to check and interpret the hyperspectral spectra. Spectral libraries are essential in the field of imaging reflectance spectroscopy for mapping purposes. For example, the spatial distribution of ore-related mineral phases can be mapped by comparing unknown reflectance pixel spectra with known reflectance material spectra from a spectral library. The data that are being analyzed are hyperspectral data cubes that are collected by, e.g., satellite, unmanned aerial vehicle (UAV) or tripod platforms to detect and map element or mineral occurrences in natural and in man-made surfaces.

The distinction of different surface materials or minerals is based on the nature of their reflectance spectral characteristics. The recorded reflectance spectral information is a function of the chemical and physical properties of the target material which cause different reactions to the incoming light on a molecular and atomic level (Clark, 1999; Hunt, 1989).

Spectral sensors collect the number of photons that are emitted or reflected per wavelengths by the material in each measured ground pixel. The interaction of the incoming light or radiant flux in a specific wavelength with the matter can reveal important information about the matter itself (Jensen, 2010). This interaction can be the absorption of a photon of a discrete energy state by an isolated atom or ion. This changes the atom's or ion's energy state. During this process energy is emitted that is not equal to the discrete energy of absorption which causes emissions at a different wavelength and creates absorption bands or absorption features (Clark, 1999; Hunt, 1989). The absorption feature position, depth and width depend on the different absorption processes taking place, the kind of chemical bond, the elements involved, and the absorbing ion or molecule and its position in the crystal lattice. Absorption features in the visible and near infrared (VNIR: 400 to 1000 nm) and shortwave infrared (SWIR: 1000 to 2500 nm) wavelength region are caused by electronic and vibrational processes within the molecule or crystal lattice. The position and cause of these reflectance absorption features are discussed in detail, e.g., in Clark (1999, 2003) and Hunt (1989).

Hyperspectral data of geological surfaces can be acquired by ground- or UAV-based outcrop scans to map an ore body's surface mineral distribution by using spectral references libraries. An example of a hyperspectral surface mapping is shown in Fig. 1. Here, the outcrop of former copper–gold–pyrite mine Apliki in the Republic of Cyprus was scanned hyperspectrally and mapped utilizing a spectral library of expected surface minerals. The analysis is based on United States Geological Survey (USGS) reflectance spectra. As the USGS spectral library entries do not originate from the same sensor as the mine face scan (HySpex data), they need to be spectrally adapted to the HySpex sensor properties.

In the case of minerals reflectance spectra, only hyperspectral sensors with a spectral bandwidth resolution of approximately 10 nm or less can capture the fine differences in reflectance at certain wavelength positions (Jensen, 2010). Future hyperspectral imaging satellites will provide the necessary data quality requirements to successfully map rare-earth elements (REEs), copper deposits and other resources from space. These satellites will play an important role in the future of geological exploration to help map large mineralized areas in remote regions (Mielke et al., 2016; Swayze et al., 2014). Several global mapping satellite missions will be launched in the next few years. Among them are the German EnMAP, the Chinese CCRSS-A and the Japanese HISUI missions (Guanter et al., 2015; Iwasaki et al., 2011; Tong et al., 2014). For those missions, the imaging spectroscopy community is currently developing methodologies, e.g., for the detection of REEs in the image spectra (Boesche et al., 2015; Boesche et al., 2017; Bösche, 2015; Herrmann, 2019; van der Meer et al., 2012; Turner et al., 2014a, b; Turner, 2015).

We aim to contribute to the already existing, accredited libraries, e.g., the USGS and the ECOSTRESS Spectral Library and various others (Baldridge et al., 2009; Clark et al., 2007; Hunt, 1977; Kokaly et al., 2017; Meerdink et al., 2019; Percival et al., 2016). The available reflectance spectral libraries are commonly based on powdered natural or synthetic samples that are spectrally pure. The spectral data are usually collected by point spectroradiometers, e.g., the Analytical Spectral Devices (ASD) FieldSpec® 3. Our contributed reflectance spectra are based on imaging spectroscopy data from the HySpex classic series scanning samples in a natural and a powdered state. Reflectance spectral libraries like the here presented, based on HySpex imaging data and untreated samples, are not yet freely available for the hyperspectral community.

The spectral and geochemical information of samples presented here belongs to three different mineral assemblages and corresponds to three different types of deposits. The sample's spectral information is provided within four spectral library files and their corresponding geochemical composition files. The four spectral library files represent (1) REE-bearing minerals, (2) synthetic REE oxide powders (Koerting et al., 2019a), (3) copper-bearing minerals (Koellner et al., 2019) and (4) powders of copper-bearing surface material from the Apliki copper–gold–pyrite mine in the Republic of Cyprus (Koerting et al., 2019b). Spectrally, the libraries cover the full wavelength range of the solar optical range (414–2498 nm). The corresponding geochemical analyses are explained in the methods for each sample type. The two REE libraries (Koerting et al., 2019a) consist of the spectra of 16 rare-earth oxide (REO) powders and 13 REE-bearing minerals (REMin). In addition, the spectra of niobium- and tantalum-oxide powders are provided, which will not be mentioned further individually but be included in the term REO. The third spectral library includes 20 copper-bearing minerals (Koellner et al., 2019), and the fourth spectral library contains 37 surface samples from the Apliki copper–gold–pyrite mine site in the Republic of Cyprus (Koerting et al., 2019b). All spectral libraries are united and comparable by the internally consistent method of hyperspectral data acquisition in the laboratory. An extensive list of the samples can be found in the technical reports provided with each dataset.

The samples are presented as reflectance spectral libraries and their geochemical composition. Sample nominations are based on the geological collection of origin or sample abbreviations from the field sampling. The sample nomination is not an interpretation of the presented geochemical data. The datasets are independent of each other, and the reflectance

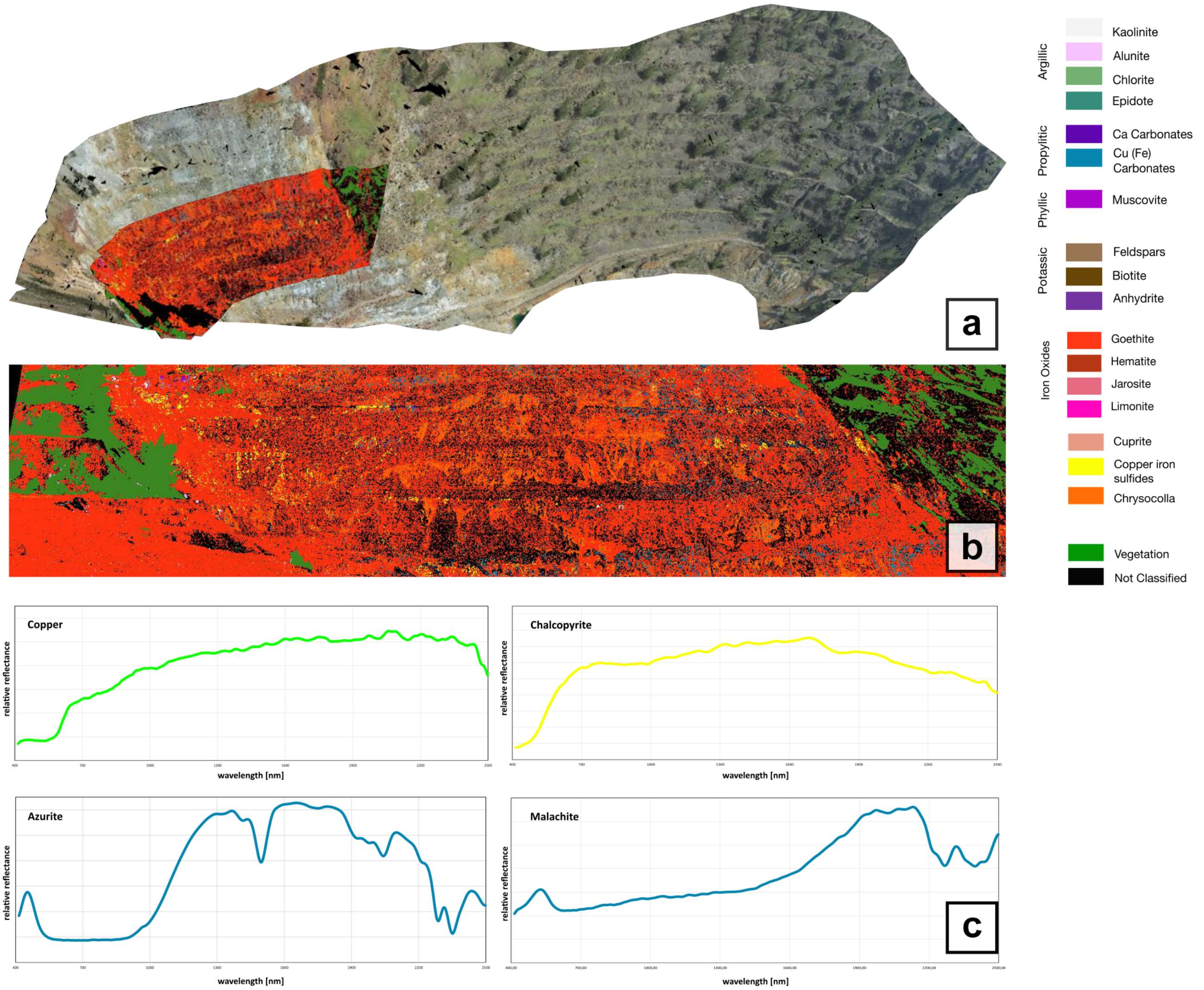

Figure 1. Example for the application of a spectral library. **(a)** Three-dimensional model of the open-pit Apliki mine in the Republic of Cyprus based on RGB images and a superimposed analysis result of a hyperspectral HySpex scan. The hyperspectral map of the spatial mineral distribution from panel **(b)** is stacked on the 3D model for visualization purposes. **(b)** Analysis of a HySpex scan using a custom-made spectral library from USGS spectra (Clark et al., 2007). **(c)** Example of hyperspectral spectra from copper-bearing minerals as presented in Koellner et al. (2019).

spectra can be seen as a spectral expression of the existing geochemical data. Neither the geochemistry nor the reflectance spectra are interpreted or correlated to each other.

The outline of this document follows the necessary line of knowledge to successfully make use of the here presented spectral libraries. Section 2 includes a description of the analyzed materials, and Sect. 3 informs about the methods, including the sample preparation and spectra collection, the hyperspectral data acquisition, covering the processing of the data and spectral measurement parameters, and the geochemical analyses of the samples. Section 4 lists the samples that were measured spectrally and geochemically and the data of which can be accessed via the GFZ Data Services platform. Section 5 discusses the parameters influencing the data. A separate data description and the geochemical analysis results are included as data reports in the three different data publications (Koellner et al., 2019; Koerting et al., 2019a, b).

2 Materials

The REE sample material includes 16 REO powders (REO) and 13 REE-bearing minerals (REMin). The REO powders belong to a series of rare-earth metals and compounds (REacton®) and were purchased from Alfa Aesar. All REO powders contained at least 99.9 % of the REE oxide, as per the seller-supplied concentration certificates. The concentration certificate information can be found in the data description of Koerting et al. (2019a). The REO powders were obtained as high-purity materials with a grain size of < 63 µm. The REMin samples (ore minerals) were purchased from Gunnar Färber Minerals, an online trader of mineral specimens. The mineral notation is based on the sample name provided by Gunnar Färber Minerals. The supplier offers analytical services with a modern scanning electron microscopy–energy-dispersive X-ray spectroscopy (SEM-EDX) technology, and therefore we assume the specimens are analyzed and the mineral species is validated before the sale. The X-ray fluorescence (XRF) data presented in the data description of Koerting et al. (2019a) should be consulted to validate the given mineral nomination noted by Gunnar Färber Minerals.

The 20 copper-bearing minerals belong to collections of the University of Potsdam (UP) and the Federal Institute for Geosciences and Natural Resources (BGR); a samples list can be found in Koellner et al. (2019). The minerals were measured hyperspectrally with no sample preparation; the sample photos and geochemical analysis are provided in the data description for Koellner et al. (2019). The 37 Apliki mine surface samples were collected (Koerting et al., 2019b) in March 2018 during a field campaign of the Geological Survey Department of the Republic of Cyprus (GSD) and the GFZ German Research Centre for Geosciences (GFZ). Surface material in the mine was collected and prepared (crushed and pulverized) for the geochemical analysis by Bureau Veritas Minerals (BVM). The powdered samples were measured hyperspectrally as powder tablets; a sample list including photos from the in situ conditions of the samples can be found in the technical report (Koerting et al., 2019b).

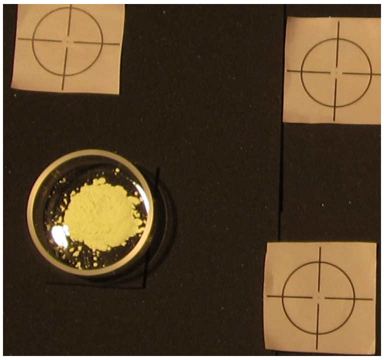

Figure 2. Holmium-oxide powder in the laboratory HySpex setting in a quartz glass petri dish underlain by black cellular rubber. Geometric markers for the pre-processing were placed alongside the sample.

Figure 3. Xenotime embedded in quartz as an example for the REE-bearing mineral samples.

3 Methods

3.1 Sample preparation and spectra collection

The sample preparation varies by sample type and depends on the material and the information of interest. This is based on the research projects that the samples stem from and for which the spectral and geochemical data were acquired.

The reflectance spectra for each sample were manually extracted from the processed hyperspectral image scenes by averaging a number of pixels over a central sample area. The resulting spectra were compiled in a spectral library. Thereby, each reflectance spectrum of a spectral library represents an average reflectance spectrum of the material, depending on the sample size and spectral homogeneity. The extraction of the reflectance spectra is explained in detail in each data description (Koellner et al., 2019; Koerting et al., 2019a, b).

The REO powders were measured in 100 % quartz glass petri dishes underlain by black cellular rubber; each powder was measured separately. Figure 2 shows the measurement setup of holmium-oxide powder as an example for the REO powders. The REE-bearing minerals were measured separately. Figure 3 shows the xenotime sample (brownish single crystal embedded in quartz) as an example for the REMin samples. The REMin samples were measured without sample preparation on black cellular rubber, as is shown for the copper-bearing minerals in Fig. 4. For all measurements, the final reflectance spectral analyses were spatially reduced to the center pixels of each identified REE-bearing mineral or a 5 pixel × 5 pixel average reflectance spectrum centered on the REO powder sample. Shadow effects from the sidewalls of the boxes could thus be minimized. One representative reflectance spectrum of every REMin and REO sample was collected for the spectral library (Herrmann, 2019).

The copper-bearing mineral samples were measured without any sample preparation as the variable surface of the minerals and the influence of the mineral structure were of interest. Figure 4 shows an example scan of some of the copper-bearing minerals. The full sample list including sample photos and the marked area of the geochemical sampling can be found in the technical report (Koellner et al., 2019). The area used to obtain the spectrum, averaging over a 5 pixel × 5 pixel window, was sampled afterwards for the geochemical analysis.

The Apliki mine samples were crushed and powdered so that ≥ 85 % of the sample was below 75 µm. Homogenized powders were measured as pressed powder tablets (Fig. 5). The area to obtain the sample's reflectance spectrum was chosen over a 5 pixel × 5 pixel window in the center of the

Figure 4. Showing HySpex scan MH_FK_LAB_Cudetect_008_09012018_WR20 as an example to highlight the lack of sample preparation.

powder tablet to minimize influences from the tablet's metal frame. The dark spots in each tablet were caused by previous measurements with a laser-induced breakdown spectrometer (LIBS). The hyperspectral sample spots were chosen in order to exclude the measurement points of the LIBS in the spectral footprint. In the case of broken powder tablets like 7d_Hem, the shadowed, rough surface areas were excluded from the spectral sampling, and an even powder surface was favored.

3.2 HySpex data recording

The HySpex VNIR-1600 and SWIR-320m-e (technical description available at http://hyspex.no/products/disc.php, last access: 18 June 2019) are two line-scanning cameras mounted in parallel. They cover the range of the visible to near infrared (VNIR, 414–993 nm) and the shortwave infrared (SWIR, 967–2498 nm) wavelength region. The sensors record an array line of 1600 pixels (VNIR) and 320 pixels (SWIR) (push-broom scanning). Every pixel contains a spectrum with a total spectral sampling number of 408 bands in total.

The HySpex cameras are provided with two acquisition modes: one for airborne data collection and one for laboratory measurements. In laboratory mode, the cameras are combined with a trigger pulse-moving sleigh (translation stage) of a definable frame period (depending on the integration time of every array-line acquisition). The configuration of the translation stage framework, the cameras and the light source (Halogen GX6.35, 2 × 1000 W, 45° illumination angle) are fixed, while the sleigh and the samples are moving through the focal plane (Rogass et al., 2017).

The reflectance level of a white reference panel, placed in line with the samples, is chosen according to the albedo of the samples. The higher the albedo of the sample, the higher is the diffuse reflectance factor of the white reference panel that is chosen. For the REE samples (REMin and REO), a white reference panel of 95 % reflectance was used because most of the REO samples were bright, white powders of a high albedo; this is based on test measurements of Bösche (2015), Herrmann (2019). The Apliki samples required a 50 % reflectance white reference panel, whereas the copper-bearing minerals were measured using a 20 % reflectance white reference panel. Both the geometrical setup and the heat-up time of the lamp influence the configuration of the light source. The maximum illumination was obtained with an angle of 45° between the incident light and the vertical plane. The distance between the lamp and the HySpex cameras was higher compared to the distance between the samples and the sensor to ensure diffuse illumination and to avoid thermal influence on the cameras and the samples. The integration time (meaning measurement time for each image line) was tested to be as high as possible to suppress the impact of signal uncorrelated Gaussian white noise and at the same time as low as needed to avoid detector saturation. For all measurements the integration time was chosen with respect to the sample albedo. The HySpex sensor characteristics are listed in Table 1. The settings used for the REMin and REOs are listed in Table 2, the settings for the copper-bearing minerals in Table 3 and the settings for the Apliki mine samples in Table 4. The laboratory is equipped with black-painted walls and doors, as well as black curtains to avoid reflected light from surfaces other than the sample; an example setup of the sensors, the translation stage and the samples can be seen in Fig. 6. The laboratory conditions were kept stable, the air temperature was regulated to 21 ± 0.5 °C and the humidity was below 70 % for all measurements. Black cellular rubber is used as a base material for all samples for hyperspectral data acquisition. It reflects less than 5 % on average of the incoming radiation.

Table 1. HySpex sensor parameters of the VNIR-1600 (VNIR) and SWIR-320m-e (SWIR).

HySpex sensor parameters		
Lamp arrangement	45°	
	VNIR	SWIR
Wavelength range [nm]	414–993	967–2498
Pixels per line	1600	320
Sampling interval [nm]	3.7	6
Radiometric resolution	12 bit	14 bit
Light source	Halogen GX6.35, 2 × 1000 W	

Detailed descriptions for the GFZ standard measurements and the process chain can be found in Rogass et al. (2017).

3.3 Hyperspectral data processing

Each measurement run produces one VNIR and one SWIR 3D data cube. The three dimensions are the two spatial x and y dimensions and the spectral z dimension. The 3D im-

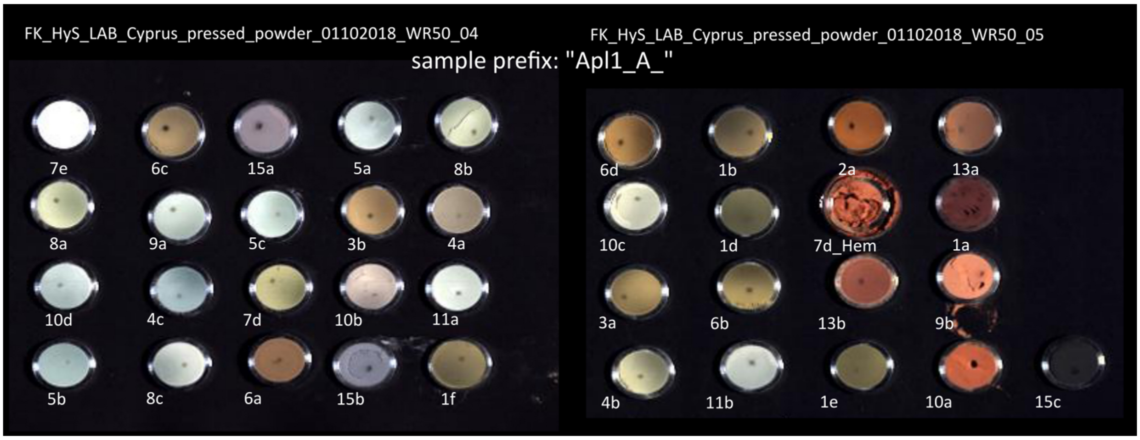

Figure 5. Showing the Apliki mine samples prepared as powder tablets.

Table 2. HySpex settings for laboratory measurements of the REO and REMin (Koerting et al., 2019a, modified following Bösche, 2015; Herrmann, 2019). "eq" stands for CCD equalization filter; "px" stands for pixels.

HySpex settings		
Distance, sample to sensor	1 m	
Sensor arrangement head to head	1 m lenses, eq on VNIR	
	VNIR (1600 px)	SWIR (320 px)
Integration time [µs]	30 000	5000
Frame period [µs]	31 000	123 506

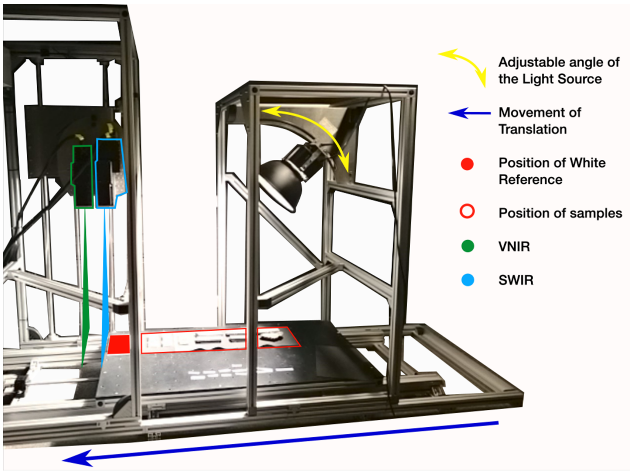

Figure 6. The HySpex translation stage setup (Körting, 2019).

age cubes are produced by moving a homogeneous reflecting white reference panel and the samples through the focal plane of the two sensors. The VNIR image cube is resized to the spatial dimensions of the SWIR data cube, coregistered and stacked with the SWIR data cube, resulting in a continuous image cube with the spectral range of 414–2498 nm. In order to produce a reflectance image, the image pixels that show the white standard were averaged to a one-line reference spectrum. The reflectance was calculated by dividing every image line spectrum by its reference spectrum from the reflecting white reference panel. The resulting reflectance data are scaled from 0–10 000. A detailed description for the laboratory setup and processing can be found in Rogass et al. (2017). The software HySpex Ground was used to perform the measurements, and the software HySpex Rad was used to perform the radiometric calibration on the image data.

3.4 Geochemical sample analysis for sample characterization

Depending on the sample type, the geochemical analysis methods differ. The methods used for each sample type are listed in Table 5.

3.4.1 Thermo Niton XL3t (XRF)

REMin

The geochemical measurements for the REMin samples were performed using an X-ray fluorescence (XRF) instrument – Thermo Niton XL3t (Fisher Scientific, 2002). The XL3t is a lightweight, hand-held XRF analyzer. The measurement principle follows the principle of X-ray fluorescence, where the sample inbound X-rays excite electrons to a higher energy level in the sample material. Energy in the form of XRF

Table 3. HySpex settings for laboratory measurements of the copper-bearing minerals (Koellner et al., 2019).

HySpex settings		
Distance, sample to sensor	30 cm	
Sensor arrangement head to head	30 cm lenses, eq on VNIR	
	VNIR (1600 px)	SWIR (320 px)
Integration time [µs]	120 000–140 000	15 000–20 000
Frame period [µs]	120 062–141 004	478 334–561 768

Table 4. HySpex settings for laboratory measurements of Apliki mine powdered samples (Koerting et al., 2019b).

HySpex settings		
Distance, sample to sensor	1 m	
Sensor arrangement head to head	1 m lenses, eq on VNIR	
	VNIR (1600 px)	SWIR (320 px)
Integration time [µs]	60 000	10 000
Frame period [µs]	60 060	239 282

Table 5. Sample type and corresponding geochemical characterization method.

Sample type	Geochemical analysis
REO (Koerting et al., 2019a)	Laboratory certificates
REMin (Koerting et al., 2019a)	X-ray fluorescence (XRF), electron probe microanalyzer (EPMA) analyses
Copper-bearing minerals (Koellner et al., 2019)	Scanning electron microscope (SEM), EPMA
Apliki mine samples (Koerting et al., 2019b)	Bureau Veritas Mineral analysis, ICP-MS and ES

radiation is released when these electrons return to their original state. The frequency of this radiation is characteristic for the measured chemical element, and its intensity is correlated to the concentration level. The intensity of each element is detected as counts per second by the detector, a geometrically optimized large area drift detector (GOLDD). The maximum excitation voltage of the XL3t device is 50 kV, which means out of the full REE suite only four light REEs can be detected (lanthanum, cerium, praseodymium and neodymium).

The XL3t spectrometer is attached to a lead-shielded sample chamber, in which samples with a diameter smaller than 3.3 cm can be placed. Mineral samples can be directly placed in the chamber; powdered samples have to be placed in sample tubes (2.5 cm diameter). The sample tubes are made of plastic with a plastic foil on the bottom. The plastic cannot be detected by XRF and therefore does not interfere with the measurements. A built-in camera of the XL3t enables the precise location of the measuring spot. The software used for the measurements is named "NDTr" and the measurement mode was "mining and exploration". The concentration levels are provided along with a balance value. "Balance" represents counts per seconds that could not be attributed to one of the measured elements. Table 6 shows the measurement modes and filters used. In-depth description of the XL3t and the XL3t results for each sample can be found in Bösche (2015) and Herrmann (2019).

Table 6. Settings used for the Thermo Niton XL3t X-ray fluorescence device (Bösche, 2015).

Thermo Niton XL3t setting	
Measurement mode	Test "all geo"
Filter	Main, low, high, light
Filter measurement time	30 s each

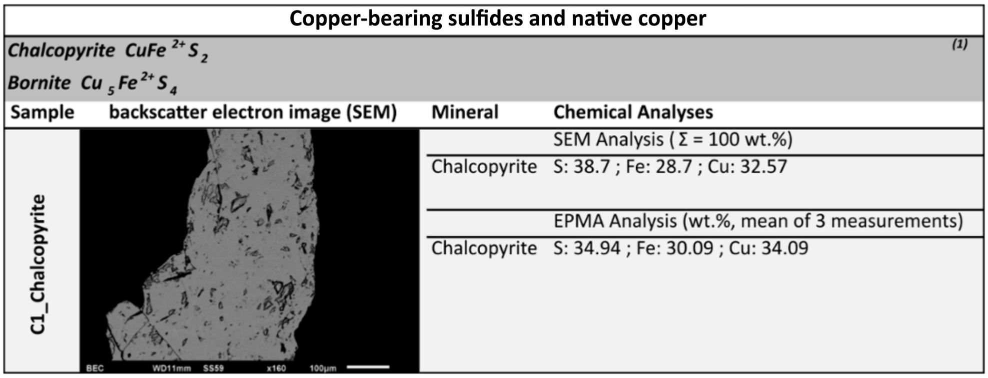

Copper-bearing sulfides and native copper

Chalcopyrite $CuFe^{2+}S_2$ (1)

Bornite $Cu_5Fe^{2+}S_4$

Sample	backscatter electron image (SEM)	Mineral	Chemical Analyses
C1_Chalcopyrite			SEM Analysis (Σ = 100 wt.%)
		Chalcopyrite	S: 38.7 ; Fe: 28.7 ; Cu: 32.57
			EPMA Analysis (wt.%, mean of 3 measurements)
		Chalcopyrite	S: 34.94 ; Fe: 30.09 ; Cu: 34.09

Figure 7. Sample C1_Chalcopyrite SEM and EPMA analysis.

Table 7. Sample C1_Chalcopyrite EPMA analysis results, from three sample points on the sample. Element concentrations reported in wt % or as below detection limit (bdl).

Sample point	Al [wt %]	Hg [wt %]	Fe [wt %]	Cu [wt %]	Si [wt %]	S [wt %]	Mn [wt %]	Total [wt %]
C1_Chalcopyrite-1	bdl	bdl	30.00	33.98	bdl	34.81	bdl	98.79
C1_Chalcopyrite-2	bdl	bdl	30.19	34.108	bdl	34.94	bdl	99.23
C1_Chalcopyrite-3	bdl	bdl	30.08	34.194	bdl	35.09	bdl	99.36

3.4.2 Scanning electron microscope (SEM) and electron probe microanalyzer (EPMA)

Copper-bearing minerals

In order to obtain information about the zonation and internal fabrics of the copper-bearing minerals, a fully automated JEOL JSM-6510 scanning electron microscope (SEM) (20 kV acceleration voltage) at the University of Potsdam was used. A back-scattered electron detector displays compositional variation in the imaging area based on the mean atomic number of the pixel. An energy dispersive X-ray spectrometer (EDX, Oxford Instruments INCAx-act) attached to the instrumentation provides quantitative elemental analysis of single spots. After calibrating with pure copper, a wide spectrum of elements can be identified. Based on previous results, divergences of up to 5 wt % can be expected, which for quantitative analysis is acceptable.

In order to approximate the values for copper a JEOL JXA-8200 electron probe microanalyzer (EPMA) at the University of Potsdam was used. The electron microprobe is equipped with five wavelength-dispersive X-ray spectrometers (WDX) and was operated with a 20 kV accelerating voltage, a 20 nA current and a beam diameter of 2 µm. The analytical counting times were 20/10 s for the element peak and 10/5 s for background positions. Analyses were calibrated using silicates/sulfides obtained from the Smithsonian Institution and Astimex. Quantifying elements of a lower atomic mass than boron is not possible; carbon cannot be measured either.

An example SEM analysis for copper-bearing mineral sample C1_Chalcopyrite can be seen in Fig. 7; the EPMA analysis of the mineral is listed in Table 7. The full SEM and EPMA results are documented in Koellner et al. (2019).

REE-bearing minerals

Some of the REMin (xenotime, bastnaesite, fluorapatite, synchysite and ilmenite) were additionally analyzed by using a JEOL JXA-8200 electron microprobe (EPMA) at the University of Potsdam based on a method developed by Lorenz et al. (2019). The conditions used for the analysis were 20 kV acceleration voltage, 20 nA beam current and a beam size of 2 µm. Counting times were between 10–20 s on peak for major elements and 50 s for REE and other trace elements.

The following spectral lines and mineral standards from Smithsonian and Astimex were used: fluorapatite (F Kα, P Kα, Ca Kα), albite (Na Kα), fayalite (Fe Kα, Mn Kα), wollastonite (Si Kα), omphacite (Al Kα), $LaPO_4$ (La Lα), $PrPO_4$ (Pr Lβ), $CePO_4$ (Ce Lα), $NdPO_4$ (Nd Lβ), YPO_4 (Y Lα), $EuPO_4$ (Eu Lα), $SmPO_4$ (Sm Lβ), $LuPO_4$ (Lu Lα), $GdPO_4$ (Gd Lα), $ErPO_4$ (Er Lβ), $DyPO_4$ (Dy Lβ), $YbPO_4$ (Yb Lα), $HoPO_4$ (Ho Lβ), uranothorite (U Mβ), and crocoite (Pb Mβ). The EPMA data were reduced using the software-implemented PRZ-XXP data-correction routine, which is based on the $\varphi(\rho z)$ method (Heinrich and Newbury, 1991).

3.4.3 Apliki mine surface sample analysis

The Apliki mine samples were analyzed by Bureau Veritas Minerals' (BVM) Canadian laboratory using their standard

Table 8. Samples, sample names and locality, and spectral library filenames of REE-bearing minerals.

Sample	Original sample name	Sample locality	Spectrum name
Aeg	Aegirine, acmite	Rundemyr, Øvre Eiker, Buskerud, Norway/TYP	REMin_Aeg
Bar	Bariopyrochlore, fluorapatite	Mina Boa Vista, Catalão, Goiás, Brazil	REMin_Bar
Bst	Bastnaesite (Ce)	Zagi Mountain, Warzal Dam, Peshawar, Khyber Pakhtunkhwa (formerly North-West Frontier Province), Pakistan	REMin_Bst
Fap	Fluorapatite, albite	Golconda Mine, Governador Valadares, Doce Valley, Minas Gerais, Brazil	REMin_Fap
Flt	Fluorite	Arbegona, Shashemanne	REMin_Flt
Gdl	Gadolinite (Y), synchysite (Y), fluorite	White Cloud Pegmatite, South Platte, Jefferson County, Colorado, USA	REMin_Gdl
Ilm	Ilmenite	Mogok, Sagaing District, Mandalay, Myanmar	REMin_Ilm
Pcr	Polycrase (Y)	Puoutevare pegmatite, Tjalmijaure Lake, Jokkmokk Lappland, Northern Sweden	REMin_Pcr
Prs	Parisite (Nd) including parisite (Ce)	Mountain Pass Mine, Ivanpah Mountains, San Bernardino County, California, USA	REMin_Prs
Syn	Synchysite (Y), microcline, quartz	White Cloud Pegmatite, South Platte, Jefferson County, Colorado, USA	REMin_Syn
Xtm1	Xenotime (Y) (a)	Novo Horizonte, Ibitiara, Bahia, Brazil	REMin_Xtm1
Xtm2	Xenotime (Y) (b)	Novo Horizonte, Ibitiara, Bahia, Brazil	REMin_Xtm2
Zrn	Zircon	Peixe Alkaline complex, Monteirópolis, Jaú do Tocantins, Tocantins, Brazil	REMin_Zrn

Table 9. Sample name and supplier, product and lot number, and spectral library filenames of the rare-earth oxide powders.

Sample name, supplier	Product number	Lot number	Spectrum name
Yttrium (III) oxide, Sigma-Aldrich	204927	MKBL2030V	REO_Yttrium
Niobium (V) oxide, Alfa Aesar	11366	L18Y022	REO_Niobium
Lanthanum (III) oxide, Alfa Aesar	11272	B08X015	REO_Lanthanum
Cerium (IV) oxide, Alfa Aesar	11372	L07S057	REO_Cerium
Neodymium (III) oxide, Alfa Aesar	11250	C02W029	REO_Neodymium
Samarium (III) oxide, Alfa Aesar	11229	61200836	REO_Samarium
Europium (III) oxide, Alfa Aesar	11299	A16Z001	REO_Europium
Gadolinium (III) oxide, Alfa Aesar	11290	A13W016	REO_Gadolinium
Terbium (III.IV) oxide, Alfa Aesar	11208	J24Q019	REO_Terbium
Dysprosium (III) oxide, Alfa Aesar	11319	61300733	REO_Dysprosium
Holmium (III) oxide, Alfa Aesar	11280	J11X030	REO_Holmium
Erbium (III) oxide, Alfa Aesar	11310	61000356	REO_Erbium
Thulium (III) oxide, Alfa Aesar	11198	F25S060	REO_Thulium
Ytterbium (III) oxide, Alfa Aesar	11191	61201069	REO_Ytterbium
Lutetium (III) oxide, Alfa Aesar	11255	G14X082	REO_Lutetium
Tantalum (V) oxide, Alfa Aesar	14709	I14Y039	REO_Tantalum

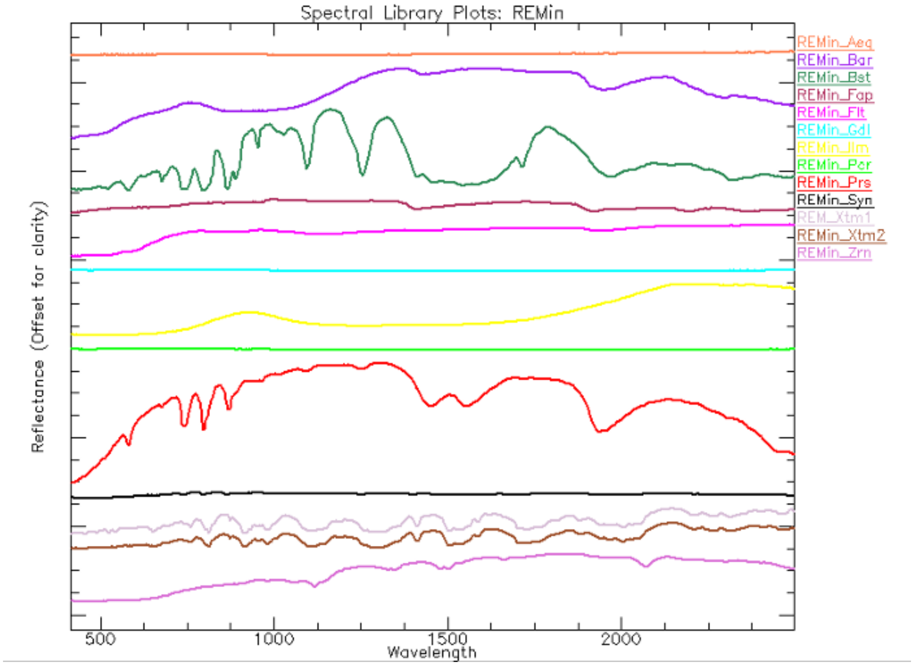

Figure 8. Spectral library plot of the REE -bearing minerals.

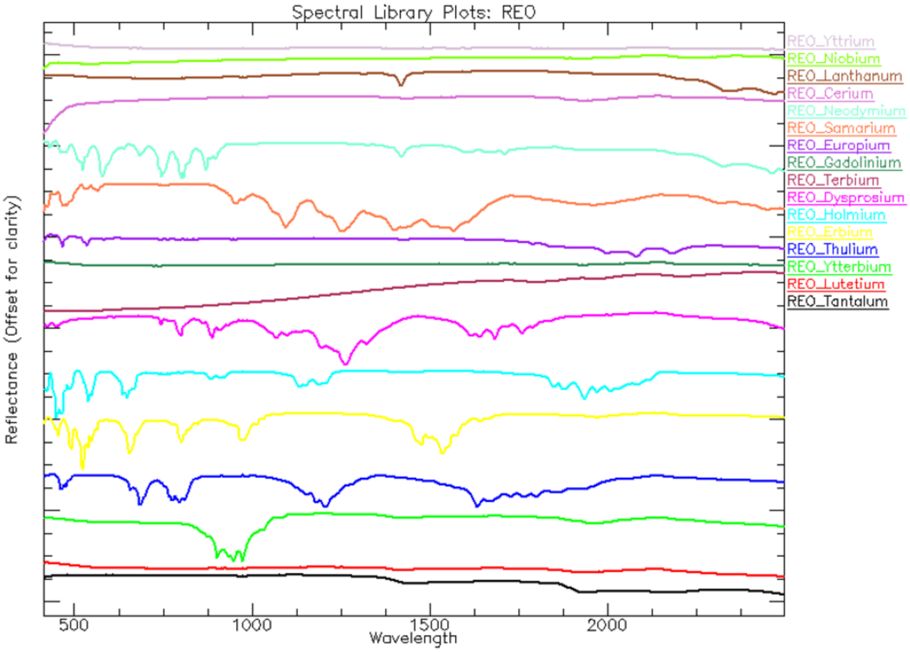

Figure 9. Spectral library plot of the rare-earth oxide powders.

packages (Bureau Veritas, 2020). The samples were pulverized below 75 µm and analyzed for major, minor and trace elements using inductively coupled plasma mass spectrometry (ICP-MS) and emission spectrometry (ICP-ES). The results are grouped by the internal BVM sample preparation/analysis method types. Those analysis method types were namely aquatic, rock and soil. The sample numbers, associated analysis method, type and internal BVM analysis codes can be found in the technical report of the Apliki mine surface sample data (Koerting et al., 2019b).

Table 10. Sample names, collection, original sample name, locality, alteration, mineral formula, spectral library filenames and geochemical composition of the copper-bearing sulfides and native copper.

Sample name	Collection	Original sample name	Sample locality	Visible alteration	Spectra names	Geochemical composition (EPMA mean, $n = 3$, wt %)
C1_Chalcopyrite	BGR	S55L16 C	Füsseberg Mine, Siegerland, Germany	strongly altered	C1_Chalcopyrite_BGR-S55L16-C [5x5 AVG]	S: 34.941; Fe: 30.091; Cu: 34.094
C2_Chalcopyrite	BGR	S115R12	Erzgebirge, Slovakia	slightly altered	C2_Chalcopyrite_BGR-S115R12 [5x5 AVG]	S: 34.903; Fe: 30.068; Cu: 33.95
C3_Chalcopyrite	BGR	S131L5 C	Henderson Mine, Clear Creek County, USA	tarnished	C3_Chalcopyrite_BGR-S131L5-C [5x5 AVG]	S: 35.039; Fe: 30.106; Cu: 33.965
C4_Chalcopyrite	UP	7534	Cornwall, England, GB	slightly altered	C4_Chalcopyrite_UP-7534 [5x5 AVG]	S: 35.007; Fe: 30.156; Cu: 34.044
C5_Chalcopyrite	UP	7526	Clausthal, Harz, Germany	altered	C5_Chalcopyrite_UP-7526 [5x5 AVG]	S: 35.053; Fe: 30.007; Cu: 34.177
K1_Copper	UP	600-1	Furnace, Lübeck, Germany	slightly altered	K1_Copper_UP-600-1 [5x5 AVG]	Cu: 98.577

4 Results

All samples are provided and described in detail in the corresponding technical reports that are available upon download of the datasets. For clarity purposes, all provided samples and corresponding spectra names are listed in Tables 8–12, including a short sample description and, where applicable, the sampling location, geochemistry or mineralogy. For each file collection a plot of the spectral library is shown (Figs. 8–13).

4.1 REE-bearing minerals and rare-earth oxide powders

The REE-bearing minerals are listed in Table 8. Figure 8 shows a plot of the corresponding spectral library. Table 9 lists the rare-earth oxide powders, and Fig. 9 shows the plot of the spectral library.

4.2 Copper-bearing minerals

The copper-bearing minerals are listed in Tables 10 (copper-bearing sulfides and native copper) and 11 (copper-bearing silicates, carbonates and sulfates). The plots of the corresponding spectral libraries are shown in Fig. 10 (copper-bearing sulfides and native copper) and 11 (copper-bearing silicates, carbonates and sulfates).

4.3 Apliki mine samples

The Apliki mine samples are listed in Table 12, and the plots of the corresponding spectral library are shown in Figs. 12 and 13.

5 Data availability

The spectral libraries are published under the Creative Commons Attribution International 4.0 License (CC BY 4.0) via GFZ Data Services. Due to the different types of samples, we present the following three data publications: (1) Mineral reflectance of 29 rare-earth minerals and rare-earth oxide powders including niobium- and tantalum-oxide powder, V. 2.0 GFZ Data Services, https://doi.org/10.5880/GFZ.1.4.2019.004 (Koerting et al., 2019a); (2) Mineral reflectance spectra and chemistry of 20 copper-bearing minerals, V. 2.0 GFZ Data Services, https://doi.org/10.5880/GFZ.1.4.2019.003 (Koellner et al., 2019) and (3) Mineral reflectance spectra and chemistry of 37 copper-bearing surface samples from Apliki copper–gold–pyrite mine in the Republic of Cyprus, V. 2.0 GFZ Data Services, https://doi.org/10.5880/GFZ.1.4.2019.005 (Koerting et al., 2019b).

6 Validation and discussion

Technical validation of the results in terms of sample material properties, systematic errors and variation of measurements (experimental error) are given below.

6.1 Sample material properties

The REO powders were certified to contain at least 99.9 % of the corresponding REO. The certificates are listed in Koerting et al. (2019a). The REE mineral samples were geochemically analyzed using the Thermo Niton XL3t (Fisher Scientific, 2002) device. The resulting element concentrations and

Table 11. Sample names, collection, original sample name, locality, alteration, mineral formula, spectral library filenames and geochemical composition of the copper-bearing silicates, carbonates and sulfates.

Sample name	Collection	Original sample name	Sample locality	Visible alteration	Spectra name	Geochemical composition (EPMA mean, $n = 3$, wt %)
A1_Azurite	UP	2458	Chéroy near Lyon, France	altered, nodular	A1_Azurite_UP-2458 [5x5 AVG]	CuO: 65.344; HgO: 0.091
A2_Azurite	UP	2437	Tsumeb near Otavi, Namibia	altered	A2_Azurite_UP-2437 [5x5 AVG]	CuO: 65.194
A3_Azurite	BGR	S101L7	Cornberg by Fulda, Germany	strongly altered	A3_Azurite_BGR-S101L7 [5x5 AVG]	CuO: 63.87; SO_3: 0.127; FeO: 0.179
B1_Brochantite	BGR	S115R3	Altenberg, Slovakia	slightly altered, powdered	B1_Brochantite_BGR-S115R3 [5x5 AVG]	Al_2O_3: 0.18; SiO_2: 0.069; SO_3: 16.262; CuO: 80.334
F1_Unknown	BGR	S115R14	Kotterbach near Witków, Poland	slightly altered	F1_Unknown_BGR-S115R14 [5x5 AVG]	SiO_2: 2.588; FeO: 69.042; CuO: 0.25; SO_3: 0.161; MnO 0.292
L1_Linarite	UP	9542	Unknown location	slightly altered, acicular	L1_Linarite_UP-9542 [5x5 AVG]	SO_3: 64.18; CuO: 24.184; HgO: 0.439
M1_Malachite	BGR	S134R8	L'Etoile du Congo Mine, Katanga, Congo	altered, nodular	M1_Malachite_BGR-S134R8 [5x5 AVG]	CuO: 67.609
M2_Malachite	BGR	S131L5 M	Henderson Mine, Clear Creek County, USA	strongly altered	M2_Malachite_BGR- S131L5-M [5x5 AVG]	CuO: 66.917
M3_Malachite	BGR	S131R4	Tsumeb near Otavi, Namibia	altered	M3_Malachite_BGR-S131R4 [5x5 AVG]	CuO: 65.176; SO_3: 0.458
M4_Malachite	BGR	S132L2	Ogonja Mine in Okahandja, Namibia	strongly altered	M4_Malachite_BGR-S132L2 [5x5 AVG]	CuO: 67.051
M5_Malachite	BGR	S55L16 M	Siegen, Germany	slightly altered, acicular	M5_Malachite_BGR-S55L16-M [5x5 AVG]	CuO: 67.885
P1_Plancheite	UP	Oberhä	Jordan	slightly altered	P1_Plancheite_UP-Oberhä [5x5 AVG]	Al_2O_3: 2.951; SiO_2: 42.079; CuO: 51.782; SO_3: 0.061; MnO: 0.243
P2_Plancheite	UP	Oberhä2	Jordan	slightly altered	P2_Plancheite_UP-Oberhä2 [5x5 AVG]	Al_2O_3: 3.727; SiO_2: 44.12; CuO: 48.902; SO_3: 0.282; MnO: 0,247
P3_Plancheite	UP	Oberhä3	Jordan	slightly altered	P3_Plancheite_UP-Oberhä3 [5x5 AVG]	Al_2O_3: 2.74; SiO_2: 43.25; CuO: 51.37; SO_3: 0.266; MnO: 0.085

the measurement error (2σ) are provided in Koerting et al. (2019a). The validation for the copper-bearing minerals can be found in Koellner et al. (2019), and the Apliki mine sample validation, analyzed by BVM, can be found in Koerting et al. (2019b).

6.2 Systematic errors of hyperspectral data acquisition

Systematic errors are discussed based on instrument drift, calibration and optimization of measurements. Initializing a warm-up phase of optical components, detectors and lamps reduced influences due to instrument drift. Additionally, laboratory conditions were monitored to ensure a stable temperature and humidity. The HySpex cameras and the reference standards are factory calibrated once per year. Measurements used for the final reflectance spectral library were collected within one calibration time span to ensure equal acquisition conditions. For HySpex, averaging multiple measurements minimizes variations in the data. An average (median) of 500 to 800 pixel reflectance spectrum was taken for the HySpex REE and REO reflectance spectra. This number relates to the maximum number of non-disturbed pixels per sample region of interest (e.g., pixels that were not shadowed from the sample holder side walls). For the copper-bearing minerals and the Apliki mine powders, a 5×5 average pixel window was chosen over the area of interest. For these samples using a smaller pixel number for the average was necessary, as the sampling of the copper-bearing minerals for geochemical

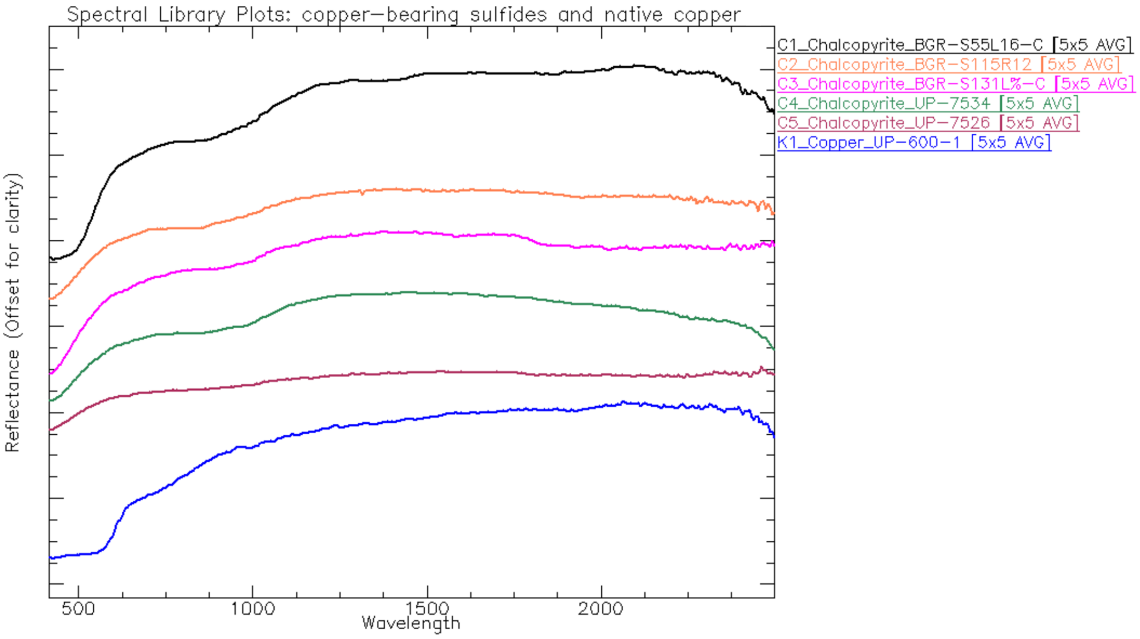

Figure 10. Spectral library plot of the copper-bearing sulfides and native copper.

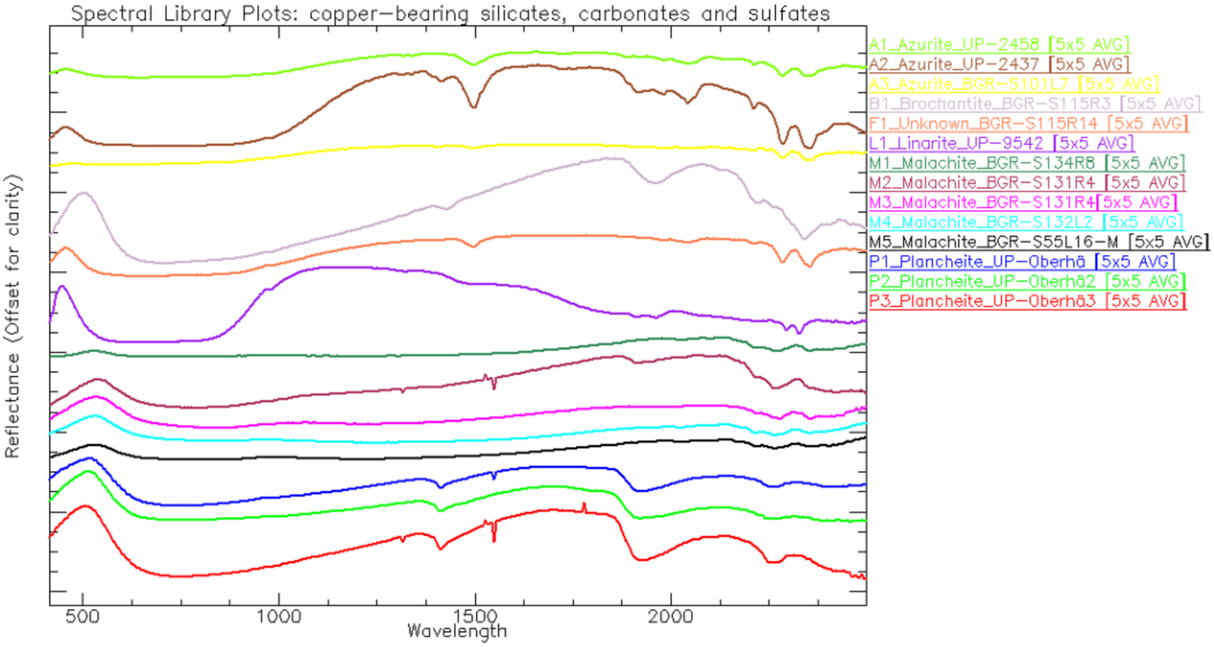

Figure 11. Spectral library plot of the copper-bearing minerals – silicates, carbonates and sulfates.

validation occurred over a small area of the sample, and the Apliki mine powder tablets were too small to ensure a larger homogenous area.

6.3 Measurements variation

Variations of measurements were not only based on instrument calibrations or drift. They can also occur due to the detector geometry or geochemical properties of the minerals. These variations may appear as a shift of the peak positions of the absorption bands. This means that different hyperspectral sensors will show variations in the spectrum of the same

Table 12. Sample names, spectral library filenames, description and mineralogy of Apliki mine sample collection.

Sample ID, “spectra name”	Description	Mineralogy based on qualitative XRD analysis (in no particular order) from Koerting (2021)
Apl1_A_1a, “Apl1_A_1a [5x5 AVG]”	Grey-green fresh surface	Not available
Apl1_A_1b, “Apl1_A_1b [5x5 AVG]”	Hematite colored weathering crust	Andesine (anorthic), quartz, magnetite, montmorillonite
Apl1_A_1d, “Apl1_A_1d [5x5 AVG]”	Fresh, dark-green weathering crust	Anorthite, magnetite, diopside, quartz, montmorillonite
Apl1_A_1e, “Apl1_A_1e [5x5 AVG]”	Yellowish orange weathering crust	Magnetite, quartz, montmorillonite, diopside, anorthite
Apl1_A_1f, “Apl1_A_1f [5x5 AVG]”	Soil formation, gravel	Magnetite, anorthite, quartz, montmorillonite, pyrite
Apl1_A_2a, “Apl1_A_2a [5x5 AVG]”	Waste, soil	Goethite, quartz, clinochlore, jarosite-natrojarosite, Andesine, gypsum
Apl1_A_3a, “Apl1_A_3a [5x5 AVG]”	Yellowish weathered, soil	Andesine (anorthic), quartz, gypsum, clinochlore, jarosite, montmorillonite
Apl1_A_3b, Apl1_A_3b [5x5 AVG]	Brownish weathered, soil	Quartz, andesine, clinochlore, gypsum, jarosite, montmorillonite
Apl1_A_4a, “Apl1_A_4a [5x5 AVG]”	White, small-grained gravel	Gypsum, quartz, clinochlore, rozenite
Apl1_A_4b, “Apl1_A_4b [5x5 AVG]”	Grey, small-grained gravel	Quartz, clinochlore, andesine, gypsum, montmorillonite
Apl1_A_4c, “Apl1_A_4c [5x5 AVG]”	Grey-green weathering crust	Quartz, clinochlore
Apl1_A_5a, “Apl1_A_5a [5x5 AVG]”	Medium-grey weathering crust	Gypsum, quartz, clinochlore
Apl1_A_5b, “Apl1_A_15b [5x5 AVG]”	Dark-grey weathering crust	Gypsum, quartz, clinochlore
Apl1_A_5c, “Apl1_A_5c [5x5 AVG]”	Light-grey weathering crust	Quartz, gypsum, clinochlore, goethite, hexahydrite
Apl1_A_6a, “Apl1_A_6a [5x5 AVG]”	Reddish brown, soil, gravel	Quartz, pyrite, analcime, goethite, montmorillonite, clinochlore, anorthite
Apl1_A_6b, “Apl1_A_6b [5x5 AVG]”	Reddish brown, soil	Anorthite, quartz, magnetite, diopside, montmorillonite, gypsum, goethite
Apl1_A_6c, “Apl1_A_6c [5x5 AVG]”	Reddish brown	Quartz, clinochlore, analcime, gypsum, calcite, jarosite, pyrite, montmorillonite
Apl1_A_6d, “Apl1_A_6d [5x5 AVG]”	Reddish brown, soil	Quartz, pyrite, anorthite, analcime, clinochlore, montmorillonite
Apl1_A_7d, “Apl1_A_7d [5x5 AVG]”	Grey, crust unstable	Quartz, hexahydrite, clinochlore, gypsum, pyrite
Apl1_A_7d_Hem, “Apl1_A_7d_Hem [5x5 AVG]”	Red, hematite	Pyrite, hematite, quartz, gypsum, clinochlore
Apl1_A_7e, “Apl1_A_7e [5x5 AVG]”	Blue crystal	Rozenite, goethite, quartz, apjohnite, ferrohexahydrite
Apl1_A_8a, “Apl1_A_8a [5x5 AVG]”	Grey, small-grained gravel	Quartz, clinochlore, pyrite, ajoite
Apl1_A_8b, “Apl1_A_8b [5x5 AVG]”	Grey, small-grained gravel	Quartz, clinochlore, pyrite, ajoite
Apl1_A_8c, “Apl1_A_8c [5x5 AVG]”	Grey, soilish,	Quartz, clinochlore, pyrite, ajoite
Apl1_A_9a, “Apl1_A_9a [5x5 AVG]”	Light-green weathering crust	Quartz, clinochlore (Mn), clinochlore
Apl1_A_9b, “Apl1_A_9b [5x5 AVG]”	Hematite vein	Quartz, clinochlore, pyrite, hematite
Apl1_A_10a, “Apl1_A_10a [5x5 AVG]”	White-with-pink weathering crust	Clinochlore, hematite, quartz
Apl1_A_10b, “Apl1_A_10b [5x5 AVG]”	White-with-purple weathering crust	Quartz, clinochlore
Apl1_A_10c, “Apl1_A_10c [5x5 AVG]”	Greenish veins	Quartz, clinochlore
Apl1_A_10d, “Apl1_A_10d [5x5 AVG]”	White evaporitic crust	Quartz, clinochlore, pyrite
Apl1_A_11a, “Apl1_A_11a [5x5 AVG]”	Grey weathering crust	Quartz, clinochlore, gypsum, bassanite
Apl1_A_11b, “Apl1_A_11b [5x5 AVG]”	Green weathering crust	Quartz, clinochlore, sphalerite
Apl1_A_13a, “Apl1_A_13a [5x5 AVG]”	Red, rock	Andesine, quartz, magnetite, montmorillonite-chlorite, diopside
Apl1_A_13b, “Apl1_A_13b [5x5 AVG]”	Red, gravel, weathered hillside rock	Clinochlore, quartz, montmorillonite
Apl1_A_15a, “Apl1_A_15a [5x5 AVG]”	Dark-blue crystalline crust	Quartz (82.6 %), Pyrite (7.5 %), Chalcopyrite (0.8 %), pentahydrate (cuprian) (9.1 %)
Apl1_A_15b, “Apl1_A_15b [5x5 AVG]”	Light-blue rock and blue crust	Quartz (86.1 %), pyrite (4.5 %), pentahydrate (cuprian) (7.1 %), covellite (2.4 %)
Apl1_A_15c, “Apl1_A_15c [5x5 AVG]”	Black pyrite	Covellite (18.9 %), quartz (39.9 %), chalcanthite (21.8 %), pyrite (20.0 %)

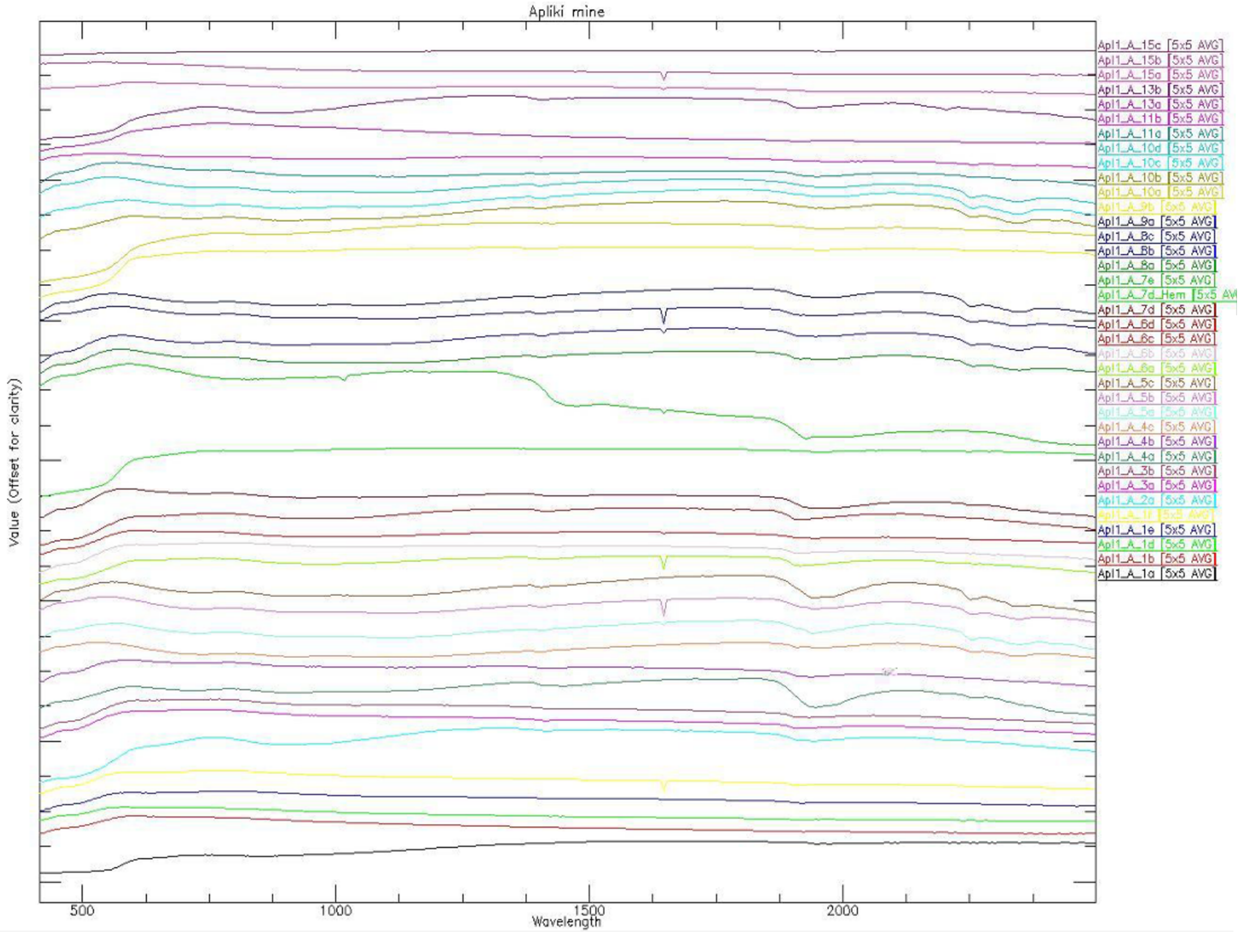

Figure 12. Spectral library of the 37 different Apliki mine samples; spectra stacked with offset.

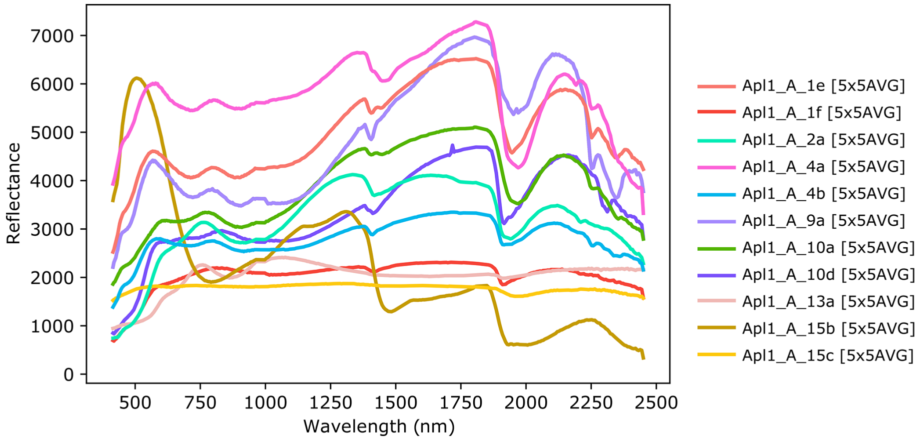

Figure 13. Detailed, unstacked view of a selection of spectra. Reflectance scaled from 0–10 000, modified from Koerting (2021).

material. By only using one set of hyperspectral sensors, the HySpex VNIR and SWIR, these shifts will not appear in our data sets. They might show when comparing our reflectance spectra of a material with reflectance spectra taken from a different instrument. For the copper-bearing minerals, the sample reflectance spectra also differ when comparing different samples of the same mineral species (e.g., malachite) to each other. The spectral signal differs, for example, due to changes in geochemistry and physical appearance, e.g., crystallization and degree of weathering (Clark, 1999; Hunt, 1989; Hunt and Ashley, 1979). To avoid measurement variations caused by different sensors, imaging data from the same sensors as the spectral library should to be used for the analysis. An example for an application can be using the here provided spectral library of the Apliki mine samples for an analysis of the HySpex hyperspectral imaging data of the Apliki mine face to be published in 2021 (Koerting et al., 2021).

6.4 XL3t systematic errors

The XL3t is internally calibrated and provides an internal warm-up phase to guarantee stable measurement conditions. Unlike the spectrometer measurements, experimental error was only provided for the XL3t. In order to reduce the experimental error, a long duration measurement time of 120 s was set. The XL3t collects the emitted radiation from the sample using four different filters. While the sample was irradiated, each filter measures counts per second within a time span of 30 s. Next, the average counts per second were internally transformed to parts per million. The irradiation of, in total, 120 s per sample was empirically tested to enable short measurement duration in combination with the lowest achievable standard deviation of concentration level.

Appendix A

Table A1. List of less commonly known terms and their abbreviations used throughout the paper.

Terms	Abbreviation	Description
Abbreviation	REE	Rare-earth element
	REO	Rare-earth oxide
	REMin	Rare-earth element-bearing mineral
	VNIR	Visible light and near infrared
	SWIR	Shortwave infrared
	XRF	X-ray fluorescence
	EnMAP	Environmental Mapping and Analysis Program: future earth observation satellite mission (http://www.enmap.org, last access: 2 March 2021)
	CCRSS-A	China Commercial Remote-sensing Satellite System: future earth observation satellite mission
	HISUI	Hyperspectral Imager Suite: future earth observation satellite mission
Instruments	HySpex VNIR-1600	HySpex push-broom spectrometer, VNIR camera
	HySpex SWIR-320m-e	HySpex push-broom spectrometer, SWIR camera
	HySpex ground	HySpex operational software for laboratory and near-field application
	HySpex rad	HySpex calibration software to transform raw digital number into radiance data
	Thermo Scientific Niton XL3t	Thermo Scientific Inc. X-ray fluorescence analyzer (NITON TM XL3t)
	NDTr	Thermo Scientific Inc. NITON TM operational software
	JEOL JXA-8200	Electron probe microanalyzer (EPMA)
	JEOL JSM-6510	Scanning electron microscope (SEM)
	Oxford Instruments INCAx-act	Energy dispersive X-ray spectrometer (EDS)
Registered brands, copyrights and/or other protected terms	REacton®	Series of rare-earth metals and compounds
	Alfa Aesar	Manufacturer and supplier of chemicals for research and development (today Thermo Scientific Inc.)
	Gunnar Färber Minerals	Supplier of mineral specimen
	REEMAP	Rare Earth Element Mapping: research project for the development of a modular multi-sensor processing chain for modern imaging spectrometers to detect REEs
	Smithsonian Institution	Smithsonian Institution Department of Mineral Sciences, reference material from the Smithsonian Microbeam Standards
	Astimex Standards Ltd.	Astimex produces standards suitable for electron probe and scanning electron microscope X-ray analysis.
	BVM	Bureau Veritas Minerals is an industry leader in the analysis of minerals for the exploration and mining industries. BVM is a service-provider company that provides mineral preparation and laboratory testing services.
Research and federal institutes	BGR	Federal Institute for Geosciences and Natural Resources
	GSD	Geological Survey Department, Ministry of Agriculture, Rural Development and Environment, Republic of Cyprus
	UP	University of Potsdam
	GFZ	German Research Centre for Geosciences
Registered trademarks	Excel™	Microsoft Excel™

Sample availability. The samples provided by the BGR are available through the collection of the BGR Spandau by their sample and collection name in the technical report (https://gewis.bgr.de/pages/MainApp.aspx?_sys_params=Nr8PDn_4fNCQfZiUX8sxJCnDDD2DVQI33NH0wD_jl45IzRSaIuClUEeLIBIzpWXeJ7K73GZUfKk, last access: 2 March 2021). The samples provided by the GFZ and UP belong to projects and have to be requested separately.

Author contributions. FK designed the Apliki-sample-related study, performed the measurements of the Apliki samples and wrote the manuscript. NK designed the copper sample study, supervised the measurements and performed the geochemical analysis at the University of Potsdam. CM and AK prepared parts of the spectral libraries. NKB designed the REE study, performed some measurements and supervised the REE measurements. SH prepared the samples and conducted most of the measurements. CR developed and applied the HySpex post-processing chain. CM and KE helped revise the manuscript. UA supervised the studies and gave valuable comments on the manuscript.

Competing interests. The authors declare that they have no conflict of interest.

Acknowledgements. We would like to thank the Helmholtz Centre Potsdam GFZ German Research Centre for Geosciences for providing the infrastructure and personnel support to conduct our research. Our gratitude also goes to the German Federal Ministry of Education and Research and the r4 subsidy program for innovative technologies for resource efficiency, which supported the REEMAP scientific project. We also want to express our gratitude to Seltenerdmetalle24, in person Manuel Schultz, for his friendly service when providing laboratory standards and negative control sample holder. Thanks to the support by the GSD we were able to conduct a study and sample in the Republic of Cyprus and our thanks go to our colleagues there for their help and directions in the unknown terrain. All the work in the Republic of Cyprus was conducted under the Permit to conduct a Geological Survey, reference no. 02.13.005.002.005.022, from 19 March 2018, granted by the Geological Survey Department, Ministry of Agriculture, Rural Development and Environment (GSD) and the director Costas Constantinou. After the termination of the permit, a memorandum of understanding (MoU) and framework for cooperation in the area of geo-science between the GSD and the GFZ was agreed upon in March 2019; the publication of the Apliki mine surface data is associated with this MoU. Constantin Hildebrand and Friederike Klos prepared parts of the spectral libraries for the data publications and contributed insight into the spectral interpretation. Pia Brinkman prepared the Apliki sample powder tablets. Marcel Horning performed most of the measurements on the copper samples and prepared the spectral copper library during his BS thesis. We thank our colleagues for their input and insights.

Financial support. This research has been supported by the Bundesministerium für Bildung und Forschung (grant no. 033R135) under the scope of the REEMAP project.

Review statement. This paper was edited by Birgit Heim and reviewed by Jeanne Percival and David Turner.

References

Baldridge, A. M., Hook, S. J., Grove, C. I., and Rivera, G.: The ASTER spectral library version 2.0, Remote Sens. Environ., 113, 711–715, https://doi.org/10.1016/j.rse.2008.11.007, 2009.

Boesche, N., Rogass, C., Lubitz, C., Brell, M., Herrmann, S., Mielke, C., Tonn, S., Appelt, O., Altenberger, U., and Kaufmann, H.: Hyperspectral REE (Rare Earth Element) Mapping of Outcrops – Applications for Neodymium Detection, Remote Sens.-Basel, 7, 5160–5186, https://doi.org/10.3390/rs70505160, 2015.

Boesche, N. K., Rogass, C., Mielke, C., Herrmann, S., Körting, F., Papenfuß, A., Lubitz, C., Brell, M., Tonn, S., and Altenberger, U.: Hyperspectral Rare Earth Element Mapping of Three Outcrops at the Fen Complex, Norway: Calcitic, Dolomitic, and Ankeritic Carbonatites, chap. 16, in: Rare Earths Industry – Technological, Economic, and Environmental Implications, Elsevier Inc., 235–265, https://doi.org/10.1016/B978-0-12-802328-0.00016-4, 2016.

Bösche, N. K.: Detection of Rare Earth Elements and Rare Earth Oxides with Hyperspectral Spectroscopy, University of Potsdam, available at: http://nbn-resolving.de/urn:nbn:de:kobv:517-opus4-85363 (last access: 2 March 2021), 2015.

Bureau Veritas: Bureau Veritas Metals, Minerals & Environmental Schedule of Services & Fees 2020, available at: http://acmelab.com/wp-content/uploads/2020/02/BV_Fees-Schedule-2020_USD_v3_07Feb2020.pdf (last access: 2 March 2021), 2020.

Clark, R. N.: Spectroscopy of rocks and minerals, and principles of spectroscopy, in: Remote sensing for the earth sciences: Manual of remote sensing, Vol. 3, 3–58, https://doi.org/10.1111/j.1945-5100.2004.tb00079.x, 1999.

Clark, R. N.: Imaging spectroscopy: Earth and planetary remote sensing with the USGS Tetracorder and expert systems, J. Geophys. Res., 108, 1–2, https://doi.org/10.1029/2002JE001847, 2003.

Clark, R. N., Swayze, G. A., Wise, R. A., Livo, K. E., Hoefen, T. M., Kokaly, R. F., and Sutley, S. J.: USGS Spectral Library splib06a: U.S. Geological Survey, Digital Data Series 231, available at: http://speclab.cr.usgs.gov/spectral.lib06 (last access: 23 June 2009), 2007.

Fisher Scientific:. Thermo Scientific NITON ™ XL3t NITON XL3t Specifications, Analysis, available at: https://www.thermofisher.com/content/dam/LifeTech/Documents/PDFs/china/Niton-XL3t-GOLDD-Spec-Sheet-2013Jan15.pdf (last access: 18 June 2019), 2002.

Guanter, L., Kaufmann, H., Segl, K., Foerster, S., Rogass, C., Chabrillat, S., Kuester, T., Hollstein, A., Rossner, G., Chlebek, C., Straif, C., Fischer, S., Schrader, S., Storch, T., Heiden, U., Mueller, A., Bachmann, M., Mühle, H., Müller, R., Habermeyer, M., Ohndorf, A., Hill, J., Buddenbaum, H., Hostert, P., Van Der

Linden, S., Leitão, P. J., Rabe, A., Doerffer, R., Krasemann, H., Xi, H., Mauser, W., Hank, T., Locherer, M., Rast, M., Staenz, K., and Sang, B.: The EnMAP spaceborne imaging spectroscopy mission for earth observation, Remote Sens.-Basel, 7, 8830–8857, https://doi.org/10.3390/rs70708830, 2015.

Heinrich, K. F. J. and Newbury, D. E. (Eds.): Electron probe quantitation, in: Microscopy Microanalysis Microstructures, Plenum Press, New York, https://doi.org/10.1051/mmm:0199200302-3029500, 1991.

Herrmann, S.: Capacity of Imaging Spectroscopy for the characterisation of REO, REE bearing minerals & primary REE-deposits, MS thesis, Scientific Technical Report; 19/08, GFZ German Research Centre for Geosciences, Potsdam, vii, 161 pp., https://doi.org/10.2312/GFZ.b103-19089, 2019.

Hunt, G. R.: Spectral signatures of particulate minerals in the visible and near infrared, Geophysics, 42, 501–513, https://doi.org/10.1190/1.1440721, 1977.

Hunt, G. R.: Spectroscopic Properties of Rocks and Minerals, in: Practical Handbook of Physical Properties of Rocks and Minerals, edited by: Carmichael, R. S., CRC Press, Cleveland, Ohio, 599–669, 1989.

Hunt, G. R. and Ashley, R. P.: Spectra of altered rocks in the visible and near infrared, Econ. Geol., 74, 1613–1629, https://doi.org/10.2113/gsecongeo.74.7.1613, 1979.

hyspex.no/products/disc.php: Norsk Elektro Optikk AS HySpex VNIR1600 and SWIR320 m-e:, available at: https://www.hyspex.no/products/disc/vnir-1600.php (last access: 18 June 2019), 2019.

Iwasaki, A., Ohgi, N., Tanii, J., Kawashima, T., and Inada, H.: Hyperspectral Imager Suite (HISUI)-Japanese hyper-multi spectral radiometer, in: International Geoscience and Remote Sensing Symposium (IGARSS), Vancouver, BC, Canada, 1025–1028, 2011.

Jensen, J. R.: Remote Sensing of the Environment An Earth Resource Perspective, 2nd Edn., Pearson Education, Darling Kindersley, South Asia, New Delhi, 2010.

Koellner, N., Koerting, F., Horning, M., Mielke, C., and Altenberger, U.: Technical Report: Mineral reflectance spectra and chemistry of 20 copper-bearing minerals, V. 2.0 GFZ Data Services, https://doi.org/10.5880/GFZ.1.4.2019.003, 2019.

Koerting, F., Herrmann, S., Boesche, N. K., Mielke, C., Koellner, N., and Altenberger, U.: Technical Report: Mineral reflectance spectra and chemistry of 29 rare-earth minerals and rare-earth oxide powders including niobium- and tantalum-oxid powder, V. 2.0 GFZ Data Services, https://doi.org/10.5880/GFZ.1.4.2019.004, 2019a.

Koerting, F., Rogass, C., Koellner, N., Horning, M., and Altenberger, U.: Technical Report: Mineral reflectance spectra and chemistry of 37 copper-bearing surface samples from Apliki copper-gold-pyrite mine in the Republic of Cyprus, V. 2.0 GFZ Data Services, https://doi.org/10.5880/GFZ.1.4.2019.005, 2019b.

Koerting, F., Koellner, N., Mielke, C., Rogass, C., Kuras, A., Altenberger, U., Klos, F., and Hildebrand, C.: Hyperspectral mine face scan of the northern open cut and laboratory scan of surface from the Apliki copper-gold-pyrite mine in the Republic of Cyprus, GFZ Data Services, in preparation, 2021.

Koerting, F. M.: Hybrid imaging spectroscopy approaches for open pit mining – Applications for virtual mine face geology, PhD thesis, University of Potsdam, 2021.

Körting, F.: Development of a 360° hyperspectral drill core scanner Test of technical conditions and validation of high-resolution near-field analysis of crystalline basement rocks using COSC-1 core samples, MS thesis, Scientific Technical Report, 19/07, GFZ German Research Centre for Geosciences, Potsdam, 97, xxi pp., https://doi.org/10.2312/GFZ.b103-19071, 2019.

Kokaly, R. F., Clark, R. N., Swayze, G. A., Livo, K. E., Hoefen, T. M., Pearson, N. C., Wise, R. A., Benzel, W. M., Lowers, H. A., Driscoll, R. L., and Klein, A. J.: USGS Spectral Library Version 7, available at: https://pubs.er.usgs.gov/publication/ds1035 (last access: 2 March 2021), 2017.

Lorenz, M., Altenberger, U., Trumbull, R. B., Lira, R., Luchi, M. L. De, Günter, C., and Eidner, S.: Chemical and textural relations of britholite- and apatite-group minerals from hydrothermal REE mineralization at the Rodeo de los Molles deposit, Central Argentina, Am. Mineral., 104,1840–1850, https://doi.org/https://doi.org/10.2138/am-2019-6969, 2019.

Meerdink, S. K., Hook, S. J., Roberts, D. A., and Abbott, E. A.: The ECOSTRESS spectral library version 1.0, Remote Sens. Environ., 230, 111196, https://doi.org/10.1016/j.rse.2019.05.015, 2019.

Mielke, C., Rogass, C., Boesche, N., Segl, K., and Altenberger, U.: EnGeoMAP 2.0—Automated Hyperspectral Mineral Identification for the German EnMAP Space Mission, Remote Sens-Basel, 8, 127, https://doi.org/10.3390/rs8020127, 2016.

Percival, J. B., Olejarz, A. D., English, M. L. R., Belley, P. M., Flynn, T., Laudadio, A. B., Stirling, J. A., and Stirling, J. A. R.: The National Mineral Reference Collection (NMC) Digital Spectral (VIS-NIR-SWIR) Library. Part I: The Kodama clay mineral collection, Geological Survey of Canada, Open File 7923, 24 pp., https://doi.org/10.4095/297564, 2016.

Rogass, C., Koerting, F. M., Mielke, C., Brell, M., Boesche, N. K., Bade, M., and Hohmann, C.: Translational imaging spectroscopy for proximal sensing, Sensors (Switzerland), 17, 1857, https://doi.org/10.3390/s17081857, 2017.

Swayze, G. A., Clark, R. N., Goetz, A. F. H., Livo, K. E., Breit, G. N., Kruse, F. A., Sutley, S. J., Snee, L. W., Lowers, H. A., Post, J. L., Stoffregen, R. E., and Ashley, R. P.: Mapping advanced argillic alteration at Cuprite, Nevada, using imaging spectroscopy, Econ. Geol., 109, 1179–1221, https://doi.org/10.2113/econgeo.109.5.1179, 2014.

Tong, Q., Xue, Y., and Zhang, L.: Progress in hyperspectral remote sensing science and technology in China over the past three decades, IEEE J. Sel. Top. Appl., 7, 70–91, https://doi.org/10.1109/JSTARS.2013.2267204, 2014.

Turner, D., Rivard, B., and Groat, L.: Rare earth element ore grade estimation of mineralized drill core from hyperspectral imaging spectroscopy, in: 2014 IEEE Geoscience and Remote Sensing Symposium, 4612–4615, 2014a.

Turner, D. J.: Reflectance spectroscopy and imaging spectroscopy of rare earth element-bearing mineral and rock samples, Doctor of Philosophy Thesis, University of British Columbia, Vancouver, April 2015.

Turner, D. J., Rivard, B., and Groat, L. A.: Visible and short-wave infrared reflectance spectroscopy of REE fluorocarbonates, Am. Mineral., 99, 1335–1346, https://doi.org/10.2138/am.2014.4674, 2014b.

van der Meer, F. D., van der Werff, H. M. A., van Ruitenbeek, F. J. A., Hecker, C. A., Bakker, W. H., Noomen, M. F., van der Meijde, M., Carranza, E. J. M., de Smeth, J. B., and Woldai, T.: Multi- and hyperspectral geologic remote sensing: A review, Int. J. Appl. Earth Obs., 14, 112–128, https://doi.org/10.1016/j.jag.2011.08.002, 2012.